View Online / Journal Homepage / Table of Contents for this issue

CrystEngComm

Dynamic Article Links

Cite this: *CrystEngComm*, 2011, **13**, 6688

www.rsc.org/crystengcomm

PAPER

Controllable synthesis of $Fe_5(PO_4)_4(OH)_3 \cdot 2H_2O$ as a highly efficient heterogeneous Fenton-like catalyst†

Di Li, Chengsi Pan, Rui Shi and Yongfa Zhu*

Received 22nd April 2011, Accepted 4th August 2011
DOI: 10.1039/c1ce05483j

$Fe_5(PO_4)_4(OH)_3 \cdot 2H_2O$ has been successfully synthesized by a simple hydrothermal process. The effects of hydrothermal temperature and pH value on the morphologies and sizes of the $Fe_5(PO_4)_4(OH)_3 \cdot 2H_2O$ particles were investigated. The $Fe_5(PO_4)_4(OH)_3 \cdot 2H_2O$ photocatalyst showed lower photocatalytic activity for the degradation of methylene blue under visible light irradiation. But the heterogeneous Fenton-like $Fe_5(PO_4)_4(OH)_3 \cdot 2H_2O$ with H_2O_2 showed highly efficient photocatalytic activity in the photocatalytic decomposition of methylene blue. Effective electron transfer from the visible light-excited dyes to Fe(III), which leads to regeneration of Fe(II) and an easy cycle of Fe(III)/Fe(II), results in much faster degradation and mineralization of methylene blue in the photo-Fenton reaction under visible light irradiation.

1. Introduction

Fenton and photo-Fenton reactions have proven to be effective methods to treat organic pollutants in wastewater, and the mechanism and kinetics have been studied by many researchers.[1–10] However, the Fenton process has significant disadvantages: iron ions have to be separated from the system at the end of the process by precipitation, which is expensive in labor, reagents and time; it is limited by a narrow pH range; and iron ions might be deactivated due to complexation with some iron complexing reagents.[11,12] To overcome these disadvantages of the homogeneous Fenton process, heterogeneous Fenton and Fenton-like catalysts have recently received much attention.

To date, investigations have mainly focused on three types of materials: an iron–oxygen series of compounds;[13–16] Fe-immobilized materials;[17–31] and natural Fe-containing materials.[32] These heterogeneous Fenton and Fenton-like catalysts were demonstrated to be useful to treat various organic pollutants in water over a wide applicable pH range. However, many of them did not show favorable catalytic activity.[12] In this sense, it is a challenging issue to develop novel heterogeneous Fenton-like catalysts with higher catalytic activity.

In this paper, $Fe_5(PO_4)_4(OH)_3 \cdot 2H_2O$ were controllably synthesized with tunable morphology by a simple hydrothermal method. The influence of reaction parameters (pH value and hydrothermal temperature) on the $Fe_5(PO_4)_4(OH)_3 \cdot 2H_2O$ morphology, structure and the relationship between the morphology and photocatalytic activity were investigated. The heterogeneous Fenton-like $Fe_5(PO_4)_4(OH)_3 \cdot 2H_2O$ with H_2O_2 showed highly efficient photocatalytic activity in the photocatalytic decomposition of methylene blue. The aim of this research was to enrich the available methods for the preparation of novel heterogeneous Fenton-like catalysts with high catalytic activity.

Department of Chemistry, Tsinghua University, Beijing, 100084, China. E-mail: zhuyf@tsinghua.edu.cn

† Electronic supplementary information (ESI) available. See DOI: 10.1039/c1ce05483j

2. Experimental section

2.1. Materials

Methylene blue of analytical reagent grade quality was used without further purification. Other chemicals were commercial products of analytical grade or reagent-grade. All the solutions were prepared with distilled water.

2.2. Preparation of $Fe_5(PO_4)_4(OH)_3 \cdot 2H_2O$

In a typical synthesis procedure, $Fe(NO_3)_3 \cdot 6H_2O$ (5 mmol) was completely dissolved in deionized water (14 ml). Under vigorous agitation, an aqueous solution (14 ml) containing $Na_3PO_4 \cdot 6H_2O$ (5 mmol) was added into the above solution at room temperature. The pH value of the mixture was adjusted with 10 M NaOH and HNO_3 (68%). Then, the mixture was transferred into a Teflon-lined steel autoclave of 40 ml, and the autoclave was heated under autogenous pressure at 180 °C for 24 h. Afterward, the autoclave was cooled to room temperature gradually. The yellowish green precipitate was washed with distilled water three times. Then, it was dried at 60 °C in air.

2.3. Characterization

The degradation rates of methylene blue (MB) solutions were scanned by a Hitachi U-3010 spectrophotometer periodically and the maximum absorption wavelength of the MB solution was identified as 664 nm. The UV-vis spectra data were recorded in the range from 200 to 800 nm. The UV-vis diffuse reflectance spectra (UV-vis DRS) of the samples were obtained on a UV-vis spectrophotometer (UV-3010, Shimadzu) using an integrating-sphere accessory. The fluorescence data were recorded on a Hitachi F-7000 Fluorescence spectrophotometer. $BaSO_4$ was used as a reflectance standard. The pH value was measured by Model PHSJ-4A pH meter. X-ray diffraction (XRD) experiments were carried out using a Rigaku DMAX-2400 diffractometer with Cu-Kα radiation. The size and morphology of $Fe_5(PO_4)_4(OH)_3 \cdot 2H_2O$ particles were characterized with the aid of a JEOL JEM-6700F field emission scanning electron microscope (SEM) and LEO-1530 field emission scanning electron microscope.

2.4. Photocatalytic oxidative degradation

The photocatalytic activities of the $Fe_5(PO_4)_4(OH)_3 \cdot 2H_2O$ were evaluated by MB decomposition under visible-light irradiation. In the case of visible-light irradiation, a 500 W xenon lamp ($\lambda >$ 290 nm, the Institute of Electric Light Sources, Beijing) was focused through a window. A 420 nm cutoff filter was placed onto the window face of the cell to ensure the desired irradiation condition. The average light intensity was 40 mW cm^{-2}. The radiant flux was measured with a power meter (the Institute of Electric Light Sources, Beijing).

A cylindrical double-layer glass photochemical reactor with internal diameter 70 mm, external diameter 80 mm, and height 80 mm was utilized for the photocatalysis reaction. A distance of about 12 cm between the lamp and reactor was maintained. Running water was piped into the layer in order to keep the temperature constant.

The photocatalytic degradation of MB in aqueous solution was studied by using $Fe_5(PO_4)_4(OH)_3 \cdot 2H_2O$ as the photocatalyst at room temperature and normal atmosphere pressure. $Fe_5(PO_4)_4(OH)_3 \cdot 2H_2O$ (50 mg) and 100 ml MB (1×10^{-5} M) aqueous solution were added into the reactor, and then stirred with a magnetic stirrer prior to irradiation by a xenon lamp at room temperature. Prior to irradiation, the solution was put in the dark for 60 min to ensure equilibrium of the working solution. After the reaction, the sample solution was put in a centrifuge to remove $Fe_5(PO_4)_4(OH)_3 \cdot 2H_2O$ from solution. The solution obtained this way was extracted into a quartz cell. The absorbance of the samples was measured using quartz cells every 60 min.

2.5. Analyses of MB intermediates

Before analysis, the samples were filtered through millipore discs of 0.45 mm to protect the chromatographic column. According to the literature,[33] the reversed-phase eluent of pH 3 buffer and methanol (65 : 35, v/v) were used for the aqueous solution. The neutral intermediates were finally identified by LC/MS (Thermo Fisher, LTQ).

2.6. Terephthalic acid fluorescence probe

It was well known that OH˙ reacts with terephthalic acid (TA) and generates TAOH which emits fluorescence at around 426 nm on the excitation of its own 312 nm absorption band.[34,35] Measurements of the amount of OH˙ were performed for the $Fe_5(PO_4)_4(OH)_3 \cdot 2H_2O$ photocatalytic reaction by means of this terephthalic acid fluorescence probe method as follows. A 100 ml aqueous solution containing 4 mmol disodium terephthalate was prepared, and then 50 mg $Fe_5(PO_4)_4(OH)_3 \cdot 2H_2O$ was suspended in 100 ml of this solution in the reactor. This was then stirred with a magnetic stirrer prior to irradiation with a xenon lamp at room temperature, and 0.1 ml H_2O_2 was added into the $Fe_5(PO_4)_4(OH)_3 \cdot 2H_2O$ suspension before stirring. After the reaction, the sample solution was put in a centrifuge to remove $Fe_5(PO_4)_4(OH)_3 \cdot 2H_2O$ from solution. The solution obtained this way was extracted into a quartz cell. The fluorescence of the samples was measured in the quartz cell every 60 min. By comparison of the fluorescence intensity with that of a known concentration of TAOH, the amount of TAOH produced was determined. The amount of OH˙ formed in $Fe_5(PO_4)_4(OH)_3 \cdot 2H_2O$ photocatalysis was estimated from that of TAOH by adopting the trapping factor.

3. Results and discussion

3.1. Controlling the synthesis of $Fe_5(PO_4)_4(OH)_3 \cdot 2H_2O$

The pH value of the starting precipitate precursors had crucial effect on the formation of $Fe_5(PO_4)_4(OH)_3 \cdot 2H_2O$. The precursor suspensions were adjusted to the desired pH values by adding NaOH solution and HNO_3 solution, and then were hydrothermally treated at 180 °C for 24 h. Fig. 1 shows the XRD patterns of $Fe_5(PO_4)_4(OH)_3 \cdot 2H_2O$ samples prepared by the hydrothermal procedure at different pH values. The diffraction peaks of all the samples could be easily indexed as a pure, orthorhombic crystalline phase $Fe_5(PO_4)_4(OH)_3 \cdot 2H_2O$, which is in good agreement with the standard card (JCPDS Card number: 45-1436). As seen from the XRD patterns, the high crystallinity could be obtained at a relatively high pH value. When the pH value was increased to 5, it changed to a mixture.

The microstructures of the as-prepared samples were then investigated with SEM. Fig. 2a shows a TEM micrograph of the sample prepared at pH = 1, from which one can see that the sample was bottle gourd in shape with diameters of 5 μm. It looks like a small sphere grew at the surface of a large sphere, and the

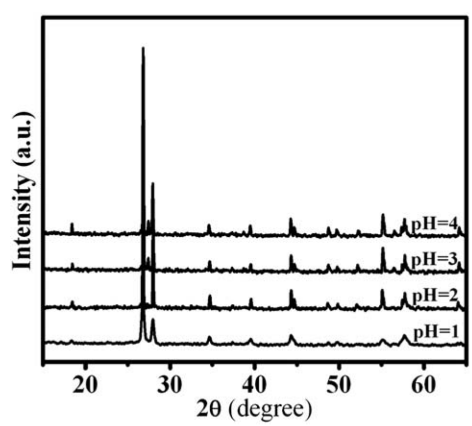

Fig. 1 XRD patterns of $Fe_5(PO_4)_4(OH)_3 \cdot 2H_2O$ samples synthesized at different pH values and treated at 180 °C.

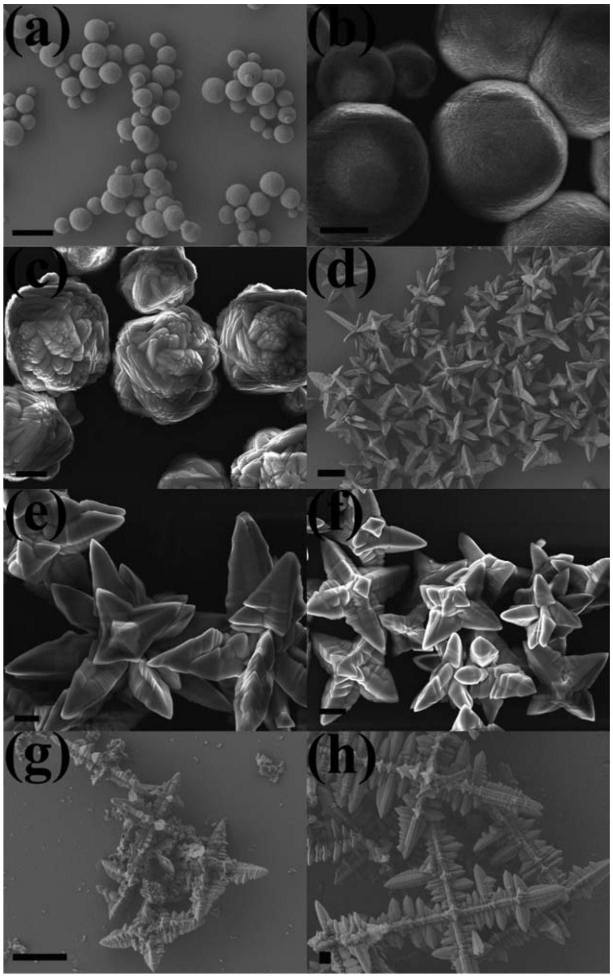

Fig. 2 Morphologies of $Fe_5(PO_4)_4(OH)_3 \cdot 2H_2O$ samples synthesized at different pHs: (a) and (b) pH = 1; (c) pH = 1.5; (d) and (e) pH = 2; (f) pH = 2.5; (g) pH = 3; (h) pH = 4. The scale bar is 10 μm in (a), (d) and (g); 2 μm in (b), (c) and (e); 3 μm in (f); 1 μm in (h).

surface of the sphere was very smooth (Fig. 2b). As the pH value was adjusted to 1.5, many horns grew on the surface of sphere (Fig. 2c). When the pH value was increased to 2, all spheres evolved into cerioid-asteroid particles with a size of 10 μm (Fig. 2d and 2e). It was like many lance-points agglomerated together. The microstructure was nearly unchanged while pH value rose to 2.5 (Fig. 2f). When the pH value was adjusted to 3 or 4, to our great surprise, many cruciate flowers existed in the resulting product (Fig. 2g and 2h). It was clear that each cruciate flower was composed of a crosslike trunk and many branches, and the branches were perpendicular to their trunk. Besides the trunk and branches, some tubers grew on the trunk and were perpendicular to branches. When the pH value was 3, there were many particles covering the surface of the cruciate flower. When the pH value increased to 4, the particles disappeared, and only pure cruciate flowers could be found. The pH value played an important role in the formation of $Fe_5(PO_4)_4(OH)_3 \cdot 2H_2O$. When the pH value was 1, there was less OH^- in solution. So the nucleation and growth of $Fe_5(PO_4)_4(OH)_3 \cdot 2H_2O$ was restrained. $Fe_5(PO_4)_4(OH)_3 \cdot 2H_2O$ grew isotropically and the morphology of $Fe_5(PO_4)_4(OH)_3 \cdot 2H_2O$ presented microspheres. As the pH value increased, the amount of OH^- also increased in the solution. The nucleation and growth of $Fe_5(PO_4)_4(OH)_3 \cdot 2H_2O$ were accelerated, so $Fe_5(PO_4)_4(OH)_3 \cdot 2H_2O$ grew anisotropically. The crystalline surface of the preferential growth direction grew faster; it caused microspheres to transform into cerioid-asteroid particles; finally the cerioid-asteroid particles turned into cruciate flowers.

On varying the reaction time with the temperature fixed at 180 °C, the $Fe_5(PO_4)_4(OH)_3 \cdot 2H_2O$ crystalline phase appeared only after 14 h hydrothermal treatment, which is shown in Fig. 3. When the $Fe_5(PO_4)_4(OH)_3 \cdot 2H_2O$ crystalline phase appeared, the cruciate flowers appeared at the same time (Fig. 4b). Before the $Fe_5(PO_4)_4(OH)_3 \cdot 2H_2O$ crystalline phase formed, only particles could be found (Fig. 4a). In addition, the temperature also had a significant influence on the formation of $Fe_5(PO_4)_4(OH)_3 \cdot 2H_2O$. When the temperature was below 160 °C, the $Fe_5(PO_4)_4(OH)_3 \cdot 2H_2O$ phase could not form (Fig. 5). The cruciate flower was broken by degrees as the temperature increased to 220 °C (Fig. 6). It meant the cruciate flower morphology could not be obtained at high temperature, as high as 220 °C, under identical solution conditions. This suggests that $Fe_5(PO_4)_4(OH)_3 \cdot 2H_2O$ might lose the water like $Ca_{10}(PO_4)_6(OH)_2$ as high as 220 °C.[36] This process was reversible, so it did not affect the properties of $Fe_5(PO_4)_4(OH)_3 \cdot 2H_2O$, but the cruciate flower morphology would be destroyed.

3.2 Optical properties and photocatalytic activity

The optical absorption of the $Fe_5(PO_4)_4(OH)_3 \cdot 2H_2O$ nanoplates was measured using a UV-vis spectrometer. The optical absorption of all the samples was nearly the same. Fig. 7 showed typical diffuse reflection spectra of $Fe_5(PO_4)_4(OH)_3 \cdot 2H_2O$ obtained after synthesis at different pH values and different temperatures. The bandgap of $Fe_5(PO_4)_4(OH)_3 \cdot 2H_2O$ obtained at different pH values are shown in Table 1. The steep shape of the spectra indicated that the visible light absorption was not due to the transition from the impurity level but was due to the bandgap transition (Table 1).[37] The band at 400–450 nm could be assigned to Fe–O charge transfer transitions.[38,39]

Methylene blue was used as a probe in the heterogeneous photocatalysis, and decoloration and decomposition could be

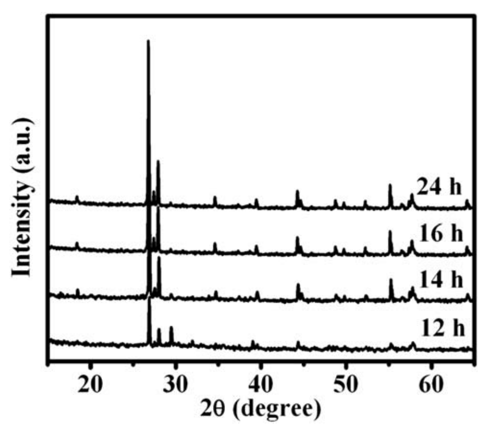

Fig. 3 XRD patterns of $Fe_5(PO_4)_4(OH)_3 \cdot 2H_2O$ samples synthesized with different reaction times and treated at 180 °C.

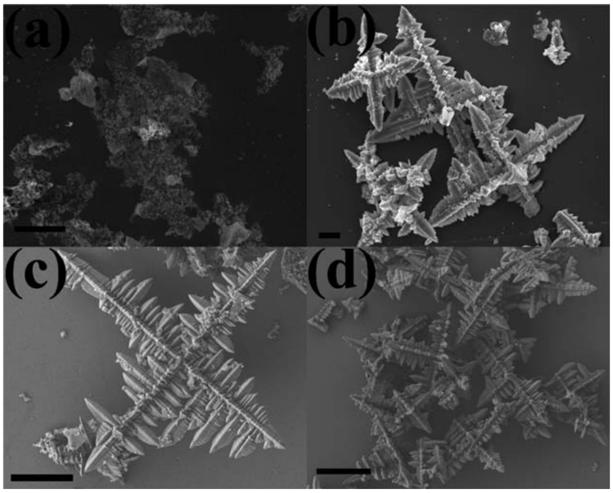

Fig. 4 Morphologies of $Fe_5(PO_4)_4(OH)_3 \cdot 2H_2O$ samples synthesized with different reaction times: (a) 12 h, (b) 14 h, (c) 16 h and (d) 24 h. The scale bar is 20 μm in (a), 3 μm in (b) and 10 μm in (c) and (d).

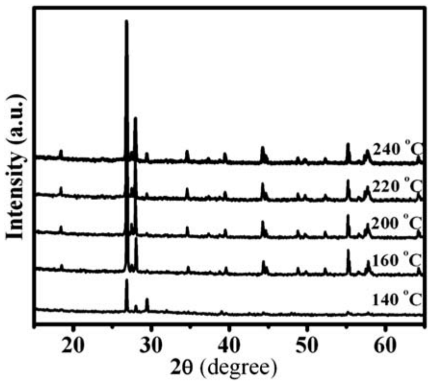

Fig. 5 XRD patterns of $Fe_5(PO_4)_4(OH)_3 \cdot 2H_2O$ samples synthesized at different temperatures and treated at pH = 4.

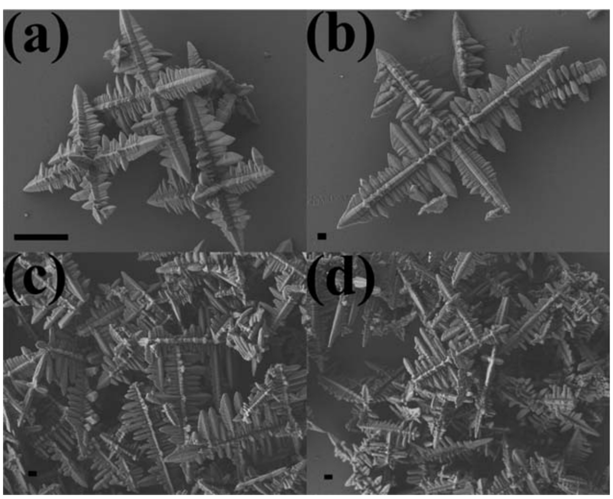

Fig. 6 Morphologies of $Fe_5(PO_4)_4(OH)_3 \cdot 2H_2O$ samples synthesized at different temperatures: (a) 160 °C; (b) 200 °C; (c) 220 °C; (d) 240 °C. The scale bar is 10 μm in (a) and 1 μm in (b), (c) and (d).

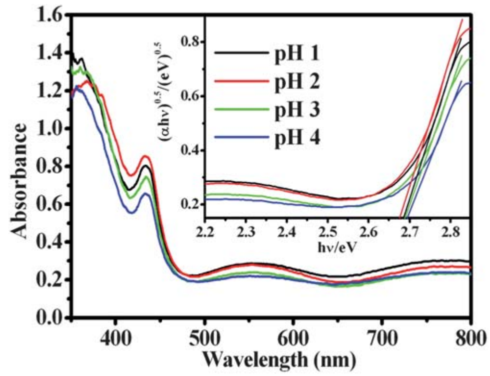

Fig. 7 UV-Vis diffuse reflectance spectra of $Fe_5(PO_4)_4(OH)_3 \cdot 2H_2O$ samples synthesized at different pH values and treated at 180 °C.

Table 1 The bandgap of $Fe_5(PO_4)_4(OH)_3 \cdot 2H_2O$ obtained at different pH values

pH value	1	2	3	4
bandgap (*hν*/eV)	2.686	2.676	2.688	2.695

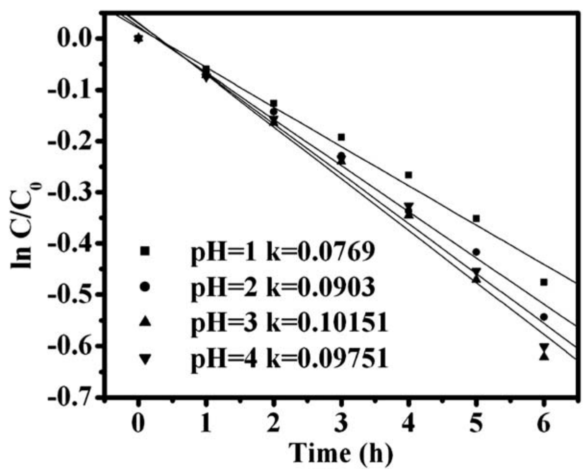

Fig. 8 First-order plots of the photocatalytic degradation of MB using $Fe_5(PO_4)_4(OH)_3 \cdot 2H_2O$ samples synthesized at different pH values.

monitored *via* the visible-light absorption signature. Fig. 8 shows the degradation of MB using the $Fe_5(PO_4)_4(OH)_3 \cdot 2H_2O$ samples synthesized at different pH values. The first-order linear relationship was revealed by plots of $\ln(C/C_0)$ *vs.* irradiation time (t), where C was the concentration of MB at the irradiation time t and C_0 was the concentration in the adsorption equilibrium of the photocatalysts before irradiation. *Via* the first order linear fit, the determined reaction-rate constants k were 0.0769, 0.0903, 0.10151 and 0.09751 h^{-1}, respectively, for the samples synthesized at different pH values. Among these samples, the photocatalytic activity increased as the pH value increased. The surface area of $Fe_5(PO_4)_4(OH)_3 \cdot 2H_2O$ obtained at different pH values is shown in Table 2. The photocatalytic activity was not in accordance with the surface area. This means the surface area has no obvious effect on the photocatalytic degradation of MB in aqueous solution. The sample obtained at low pH was not highly

Table 2 The BET results of $Fe_5(PO_4)_4(OH)_3 \cdot 2H_2O$ obtained at different pH values

pH value	1	2	3	4
BET surface area/m^2 g^{-1}	23.31	0.27	0.75	1.65

Table 3 The BET results of $Fe_5(PO_4)_4(OH)_3 \cdot 2H_2O$ obtained at different temperatures

Temperature/°C	180	200	220	240
BET surface area/m^2 g^{-1}	1.65	1.08	1.27	0.51

crystalline, which was confirmed by the XRD result. A lot of defects could act as an electron–hole recombination center, resulting in a low photocatalytic activity. Fig. 9 shows the first-order plots for the photocatalytic degradation of MB using $Fe_5(PO_4)_4(OH)_3 \cdot 2H_2O$ samples synthesized at different temperatures. The reaction rate constant k was 0.09233, 0.10318, 0.08909, 0.09751 and 0.10942 h^{-1}, respectively, for the 240, 220, 200, 180 and 160 °C samples. The surface area of $Fe_5(PO_4)_4(OH)_3 \cdot 2H_2O$ obtained at different temperatures is shown in Table 3. The surface area of $Fe_5(PO_4)_4(OH)_3 \cdot 2H_2O$ obtained at different temperatures was similar. This means the temperature has no obvious effect on the surface area. When the pH value was 4, the activity of the sample prepared at 160 °C was the highest. The photocatalytic activity was not in accordance with surface area. It was mainly attributed to a better crystalline phase which was consistent with the XRD.

3.3. Photocatalytic activity of the Fenton-like reaction and the reaction mechanism

The degradation process of MB catalyzed by $Fe_5(PO_4)_4(OH)_3 \cdot 2H_2O$ obtained at 160 °C with various H_2O_2 concentrations is shown in Fig. 10. The first-order linear relationship was obtained, as showed by the plots of ln(C/C_0) *versus* reaction time (the inset of Fig. 10). The reaction rate constant k was 0.34252, 0.40664, 0.27864 and 0.37608 h^{-1} for 4.9 mM, 9.8 mM, 14.7 mM and 19.6 mM H_2O_2 concentrations, respectively. The optimal H_2O_2 concentration was 9.8 mM. The reaction rate was far higher than without H_2O_2. It belongs to a Fenton-like reaction. It was found that due to effective electron transfer from the visible light-excited dyes to Fe(III), which leads to regeneration of Fe(II) and an easy cycle of Fe(III)/Fe(II), much faster degradation and mineralization of various dyes was achieved in the photo-Fenton reaction under visible light irradiation.[40–43] The mechanism of the Fenton-like reaction is shown in Scheme 1.[44,45]

Fig. 10 also shows that the spectral band at 664 nm blue-shifts during the course of the photodegradation. As weak electron-donor substituents, methyl groups could facilitate attack on MB by OH˙ in the demethylation process; this is also likely to be a major step in the photocatalytic oxidative degradation of MB.[46] Examination of the spectral variations in Fig. 10 suggest that MB is *N*-demethylated in a stepwise manner (methyl groups are removed one at a time as confirmed by the gradual peak wavelength shifts toward the blue region), with cleavage of the MB chromophore ring structure occurring concomitantly. *N*-demethylation, deamination and oxidative degradation takes place during the photocatalyzed degradation of MB.[46] Mixtures of *N*-demethylated intermediates yield spectra with broad absorption bands in the visible range. To examine the process in detail, the neutral intermediates were also identified by LC/MS (Fig. S1†). The suggested structures of the intermediates based on the LC/MS results are shown in Table 1 of the supporting information.† The result is consistent with the UV-vis spectral result.

Fig. 11 shows the fluorescence spectra observed for a solution of the $Fe_5(PO_4)_4(OH)_3 \cdot 2H_2O$ suspension containing 16 mM disodium terephthalate irradiated for various duration times. Since the observed fluorescence spectra were identical to that of TAOH, it was concluded that TAOH was generated from TA by the reaction with OH˙,[47] where OH˙ was formed in the $Fe_5(PO_4)_4(OH)_3 \cdot 2H_2O$ photocatalysis. Fig. 11 represents the fluorescence intensity as a function of the duration of irradiation. Since the fluorescence intensity increases with irradiation time until 5 h of visible light irradiation, the amount of OH˙ formed in the $Fe_5(PO_4)_4(OH)_3 \cdot 2H_2O$ photocatalysis reaches an equilibrium after this duration under visible light irradiation.

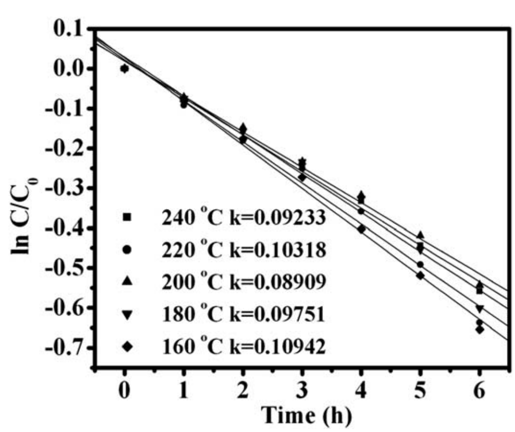

Fig. 9 First-order plots of the photocatalytic degradation of MB using $Fe_5(PO_4)_4(OH)_3 \cdot 2H_2O$ samples synthesized at different temperatures.

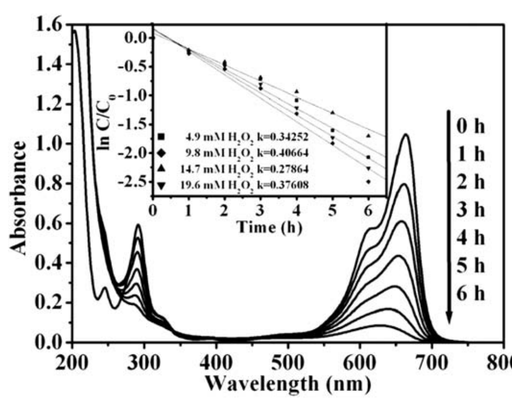

Fig. 10 The UV-vis spectral changes of MB ($Fe_5(PO_4)_4(OH)_3 \cdot 2H_2O$: 0.5 g l^{-1}; H_2O_2: 9.8 mM; MB: 1 × 10^{-5} M). Inset: the first-order linear relationship for the photocatalytic degradation of MB using various H_2O_2 concentrations.

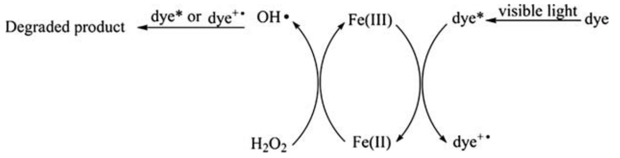

Scheme 1 The mechanism of the Fenton-like reaction.

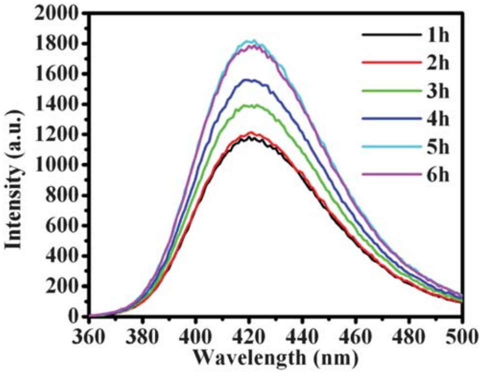

Fig. 11 The changes in the fluorescence spectra of the irradiated $Fe_5(PO_4)_4(OH)_3\cdot 2H_2O$ (0.5 g L^{-1}) suspension containing 40 mM disodium terephthalate and 9.8 mM H_2O_2 at various irradiation periods.

4. Conclusions

In conclusion, the photocatalytic properties of $Fe_5(PO_4)_4(OH)_3\cdot 2H_2O$ were investigated under visible light irradiation in detail. The $Fe_5(PO_4)_4(OH)_3\cdot 2H_2O$ was first tested and used as a heterogeneous Fenton-like catalyst. It was found that $Fe_5(PO_4)_4(OH)_3\cdot 2H_2O$ possessed high catalytic activity towards the degradation of MB in the presence of H_2O_2. The high catalytic activity could be attributed to an interesting mechanism, that is, the activation of H_2O_2 by Fe(III) in $Fe_5(PO_4)_4(OH)_3\cdot 2H_2O$ by a Fenton-like pathway.

Acknowledgements

This work is supported by Chinese National Science Foundation (20925725 and 50972070) and National Basic Research Program of China (2007CB613303).

References

1 R. G. Zepp, B. Faust and J. Hoigne, *Environ. Sci. Technol.*, 1992, **26**, 313.
2 T. Brinkmann, P. Horsch, D. Sartorius and F. H. Frimmel, *Environ. Sci. Technol.*, 2003, **37**, 4190.
3 W. Gernjak, T. Krutzler, A. Glaser, S. Malato, J. Caceres, R. Bauer and A. R. Fernández-Alba, *Chemosphere*, 2003, **50**, 71.
4 H. J. H. Fenton, *J. Chem. Soc.*, 1894, **6**, 899.
5 C. Walling, *Acc. Chem. Res.*, 1975, **8**, 125.
6 A. Kunai, S. Hata, Sotaro Ito and K. Sasaki, *J. Am. Chem. Soc.*, 1986, **108**, 6012.
7 C. Walling, *Acc. Chem. Res.*, 1998, **31**, 155.
8 S. Goldstein and D. Meyerstein, *Acc. Chem. Res.*, 1999, **32**, 547.
9 J. J. Pignatello, D. Liu and P. Huston, *Environ. Sci. Technol.*, 1999, **33**, 1832.
10 B. Ensing, F. Buda, P. Blochl and J. E. Baerends, *Angew. Chem., Int. Ed.*, 2001, **40**, 2893.
11 E. V. Kuznetsova, E. N. Savinov, L. A. Vostrikova and V. N. Parmon, *Appl. Catal., B*, 2004, **51**, 165.
12 S. Caudo, G. Centi, C. Genovese and S. Perathoner, *Top. Catal.*, 2006, **40**, 207.
13 J. Bandara, J. A. Mielczarski and J. Kiwi, *Appl. Catal., B*, 2001, **34**, 321.
14 S. Chou and C. Huang, *Chemosphere*, 1999, **38**, 2719.
15 R. C. C. Costa, M. F. F. Lelis, L. C. A. Oliveira, J. D. Fabris, J. D. Ardisson, R. R. V. A. Rios, C. N. Silva and R. M. Lago, *J. Hazard. Mater.*, 2006, **B129**, 171.
16 R. C. C. Costa, F. C. C. Moura, J. D. Ardisson, J. D. Fabris and R. M. Lago, *Appl. Catal., B*, 2008, **83**, 131.
17 S. Parra, L. Henao, E. Mielczarski, J. Mielczarski, P. Albers, E. Suvorova, J. Guindet and J. Kiwi, *Langmuir*, 2004, **20**, 5621.
18 S. Parra, V. Nadtotechenko, P. Albers and J. Kiwi, *J. Phys. Chem. B*, 2004, **108**, 4439.
19 M. R. Dhananjeyan, E. Mielczarski, K. R. Thampi, Ph. Buffat, M. Bensimon, A. Kulik, J. Mielczarski and J. Kiwi, *J. Phys. Chem. B*, 2001, **105**, 12046.
20 Y. Flores, R. Flores and A. A. Gallegos, *J. Mol. Catal. A: Chem.*, 2008, **281**, 184.
21 X. Tao, J. Su, L. Wang and J.-F. Chen, *J. Mol. Catal. A: Chem.*, 2008, **280**, 186.
22 J. H. Ramirez, F. J. Maldonado-Hódar, A. F. Pérez-Cadenas, C. Moreno-Castilla, C. A. Costa and L. M. Madeira, *Appl. Catal., B*, 2007, **75**, 312.
23 M. M. Cheng, W. H. Ma, J. Li, Y. P. Huang, J. C. Zhao, Y. X. Wen and Y. M. Xu, *Environ. Sci. Technol.*, 2004, **38**, 1569.
24 Y. Zhao and J. Hu, *Appl. Catal., B*, 2008, **78**, 250.
25 M. Noorjahan, V. Durga Kumari, M. Subrahmanyam and L. Panda, *Appl. Catal., B*, 2005, **57**, 291.
26 T. Yuranova, L. Garamszegi, Jan-Anders Manson, M. Bensimon and J. Kiwi, *J. Photochem. Photobiol., A*, 2002, **150**, 195.
27 F. Martínez, G. Calleja, J. A. Melero and R. Molina, *Appl. Catal., B*, 2007, **70**, 452.
28 J. Feng, X. Hu and P. L. Yue, *Water Res.*, 2006, **40**, 641.
29 J. H. Ramirez, C. A. Costa, L. M. Madeira, G. Mata, M. A. Vicente, M. L. Rojas-Cervantes, A. J. López-Peinado and R. M. Martín-Aranda, *Appl. Catal., B*, 2007, **71**, 44.
30 M. Bobu, A. Yediler, I. Siminiceanu and S. Schulte-Hostede, *Appl. Catal., B*, 2008, **83**, 15–23.
31 I. Muthuvel and M. Swaminathan, *Catal. Commun.*, 2007, **8**, 981.
32 W. F. de Souza, I. R. Guimarães, L. C. A. Oliveira, M. C. Guerreiro, A. L. N. Guarieiro and K. T. G. Carvalho, *J. Mol. Catal. A: Chem.*, 2007, **278**, 145.
33 J. D. Donaldson, S. M. Grimes, N. G. Yasri, B. Wheals, J. Parrick and W. E. Errington, *J. Chem. Technol. Biotechnol.*, 2002, **77**, 756.
34 J. T. Mason, P. J. Lorimer, M. D. Bates and Y. Zhao, *Ultrason. Sonochem.*, 1994, **S91**, 1.
35 A. W. Armstrong, A. R. Facey, W. D. Grant and G. W. Humphreys, *Can. J. Chem.*, 1963, **41**, 1575.
36 J. Cihlář, A. Buchal and M. Trunec, *J. Mater. Sci.*, 1999, **34**, 6121.
37 A. Kudo, I. Tsuji and H. Kato, *Chem. Commun.*, 2002, 1958.
38 P. Nagaraju, Ch. Srilakshmi, N. Pasha, N. Lingaiah, I. Suryanarayana and P. S. Sai Prasad, *Appl. Catal., A*, 2008, **334**, 10.
39 P. Nagaraju, N. Lingaiah, M. Balaraju and P. S. Sai Prasad, *Appl. Catal., A*, 2008, **339**, 99.
40 K. Wu, T. Zhang, J. Zhao and H. Hidaka, *Chem. Lett.*, 1998, 857.
41 K. Wu, Y. Xie, J. Zhao and H. Hidaka, *J. Mol. Catal. A: Chem.*, 1999, **144**, 77.
42 F. Herrera, J. Kiwi, A. Lopez and V. Nadtocheko, *Environ. Sci. Technol.*, 1999, **33**, 3145.
43 M. Cheng, W. Ma, J. Li, Y. Huang, J. Zhao, Y. Wen and Y. Xu, *Environ. Sci. Technol.*, 2004, **38**, 1569.
44 J. Ma, W. Song, C. Chen, W. Ma, J. Zhao and Y. Tang, *Environ. Sci. Technol.*, 2005, **39**, 5810.
45 J. Deng, J. Jiang, Y. Zhang, X. Lin, C. Du and Y. Xiong, *Appl. Catal., B*, 2008, **84**, 468.
46 T. Zhang, T. Oyama, A. Aoshima, H. Hidaka, J. Zhao and N. Serpone, *J. Photochem.Photobiol., A*, 2001, **140**, 163.
47 T. Hirakawa and Y. Nosaka, *Langmuir*, 2002, **18**, 3247.